IChemE

www.icheme.org/journals
doi: 10.1025/cherd.05069

0263–8762/06/$30.00+0.00

Trans IChemE, Part A, January 2006
Chemical Engineering Research and Design, 84(A1): 38–46

LONG-TIME SOLIDS SUSPENSION SIMULATIONS BY MEANS OF A LARGE-EDDY APPROACH

J. J. DERKSEN*

Kramers Laboratorium voor Fysische Technologie, Delft University of Technology, Delft, The Netherlands

Large-eddy simulations (LES) have been used to study solids dispersion in an unbaffled, tall, turbulently stirred tank equipped with four A310 impellers. Experiments show that in such tanks particles that are heavier than the fluid tend to rise slowly to the top of the tank (Pinelli *et al.*, 2001). The time span of this process (of the order of 20 min, or 20 000 impeller revolutions) makes a concurrent simulation of flow and particle motion unpractical. We propose a method that allows for long-time simulations and makes use of the highly resolved (in space and time) information contained in the LES. In the method, the solid particles are tracked through a series of previously stored fluid flow fields. The results are encouraging, showing indeed the observed, counterintuitive behaviour of the particles with the correct time scale. The simulated steady-state particle concentration profiles are, however, significantly sharper than their experimental counterparts, due to the schematizations involved, and possibly the underestimation of the subgrid-scale velocities.

Keywords: stirred tank flow; large-eddy simulation; turbulence; solids suspension; long-time behaviour; CFD.

INTRODUCTION

Large-eddy simulations (LES) of strongly turbulent fluid flows have great potential in mixing research and related fields of chemical engineering. In the first place because they allow for accurate predictions of flows in complex confinements such as stirred tanks (Derksen and Van den Akker, 1999; Derkson, 2001; Bakker and Oshinowo, 2004). This accuracy is not only reflected by the way the average flow field is represented, but also by the fluctuation levels, and the temporal behaviour of (macro) instabilities (Derksen and Van den Akker, 2000; Roussinova *et al.*, 2003; Hartmann *et al.*, 2004). In the second place, LES provides detailed, temporally resolved flow-field information. Such information is vital in many examples of process modelling: local, time-resolved values of the rate at which turbulent kinetic energy is dissipated determine the occurrence of droplet break-up events (Kraume *et al.*, 2004); orthokinetic agglomeration in industrial crystallizers is due to shear rates at the scale of the crystals in turbulent flow (Hollander *et al.*, 2001); in chemically reacting flows, micro-mixing frequencies determine the rate at which homogenization takes place at the smallest scales of scalar transport (Van Vliet *et al.*, 2005). The relations between the turbulence quantities (such as the energy dissipation rate ε), and the physico-chemical processes at the micro-scale are very often of a non-linear nature, which explains the need for spatially and temporally resolved data (the average value of a non-linear function of ε is different from the same function evaluated for the (time and/or space) average value of ε).

The price that is paid for the LES results is a large computational effort: the grid should be sufficiently fine to have (more or less) universal behaviour at the subgrid-scales, the method is intrinsically three-dimensional and time-dependent, and no geometrical symmetries can be utilized to limit the size of the computational domain. This is not so much of a problem when the aim is to solely simulate the flow field. In general, converged statistics of stirred tank flow can be obtained by simulating the flow for a time equivalent of 10 to 30 impeller revolutions which can be realized in a matter of days (provided that the flow does not show low-frequency, unstable behaviour; then the extent of the simulation should be at least one order of magnitude more, see e.g., Hartmann *et al.*, 2004). There is, however, a problem when the LES has to supply data for slow (micro-scale) processes. If these processes evolve on a time-scale much larger than the macro time-scale of the flow (a typical value for the latter is the period of one impeller revolution), the concurrent simulation of the flow and the other processes is hardly an option, simply because the LES would take too much

*Correspondence to: Dr J. J. Derksen, Kramers Laboratorium voor Fysische Technologie, Delft University of Technology, Prins Bernhardlaan 6, 2628 BW, Delft, The Netherlands.
E-mail: jos@klft.tn.tudelft.nl

computer time. Examples of such long-time processes are those involving liquid–liquid dispersions (Baldyga *et al.*, 2001), and crystallization (Kramer and Jansens, 2003). In special cases, however, one can apply LES results in all their detail to predict turbulence-related processes that span very many macro time-scales (in this article of the order of 10^4 impeller revolutions).

The case that we discuss in this article is related to solid particle transport in a tall, unbaffled stirred tank equipped with four hydrofoil Lightnin A310 impellers. Experiments on this case have been reported by Pinelli *et al.* (2001). They show intriguing behaviour of the particulate phase: particles that initially were all lying on the bottom of the tank gradually rose to the top of the tank after the agitation was started. It took about 20 min before a quasi steady-state particle distribution was reached, with most particles in the upper part of the tank. With an agitation speed of 16.6 rev/s, 20 min corresponds to approximately 20 000 impeller revolutions. Capturing this behaviour was the initial motivation for the work presented here. A more generic aim that we pursue is to show what strategies can be followed, and what obstacles are encountered before one can apply LES data (necessarily collected over a limited amount of process time) to study long-time processes.

The article is organized in the following manner: in the next section the flow system is defined, the LES method is explained, and single-phase LES results are presented. Then we move on to the two-phase (solid–liquid) flow and briefly describe the experimental observations. Subsequently, the method for employing the single-phase LES results for studying long-time particle motion is discussed, along with an extensive check of the consistency of the method. Finally, results are compared with the experimental observations by Pinelli *et al.* (2001), and conclusions are drawn.

SINGLE-PHASE FLOW SYSTEM

In the article by Pinelli *et al.* (2001) solids dispersion in various tall tanks with multiple impellers was considered. The configurations all had a height (H) over diameter (T) aspect ratio of 4, and were equipped with four equally spaced impellers. Montante *et al.* (2001) numerically studied the case of four pitched blade impellers revolving in a baffled tank. In this article, we will consider the case of an unbaffled tank with hydrofoil Lightnin A310 impellers. The tank geometry is shown in Figure 1. Note that at the top surface a no-slip boundary condition applies, since the liquid is covered with a lid. In the experiments, the tank diameter was $T = 23.6$ cm. With $N = 16.6$ rev/s, $D = 9.6$ cm, and $\nu = 0.9 \times 10^{-6}$ m^2 s^{-1} the Reynolds number is $Re = 1.6 \times 10^5$. As a result, we expect strongly turbulent flow.

The procedure to simulate the single-phase flow in the vessel is very similar to the one that has been described in detail by Derksen and Van den Akker (1999). The only difference being that the standard Smagorinsky subgrid-scale model (Smagorinsky, 1963) is now supplemented with wall-damping functions to bring the eddy viscosity explicitly to zero at solid walls (this to mimic physical reality in which the velocity fluctuations, and therefore the subgrid-stresses are zero at the walls). Especially in case of strongly swirling flows, incorporation of wall-damping is essential to get accurate results (Derksen, 2005).

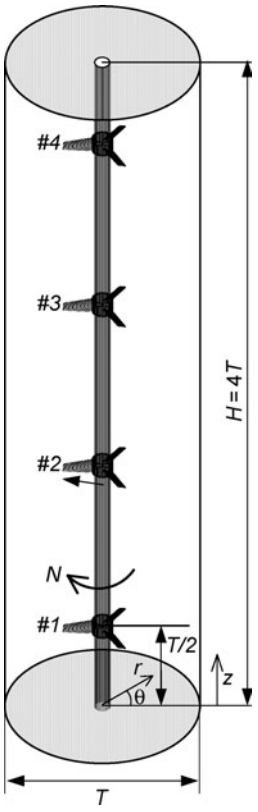

Figure 1. Flow geometry and (r, z, θ) coordinate system. The impeller rotates in the negative θ-direction and therefore pumps in the downward direction.

The Navier–Stokes equations were discretized on a uniform, cubic grid by means of the lattice-Boltzmann method (Chen and Doolen, 1998). The spatial resolution was such that the tank diameter spanned 200 grid-spacings ($T = 200\Delta$). The tank wall and impeller were represented by sets of control points on which the prescribed velocities due to the no-slip condition were imposed by means of the adaptive force-field technique (Derksen and Van den Akker, 1999). The temporal resolution was such that one impeller revolution took 2400 time steps ($\Omega \equiv 2\pi N = 2\pi/2400\ \Delta t$).

It is well known that turbulent flows with a strong swirl component very slowly evolve towards a quasi-steady state (Derksen, 2005). In order to quickly proceed to a developed flow, we started with one-quarter of the total geometry (a single impeller in a tank with $H = T$) and brought that to quasi-steady state. In two steps (via one half of the geometry) we extended the geometry to its full extent. Monitoring the phase-average flow in a vertical plane through the tank's center learned that after 60 impeller revolutions in the full geometry a quasi-steady state was reached. The subsequent 37 impeller revolutions were used to store time-dependent flow information for the particle motion part of the simulations that will be discussed in the next section.

An overall picture of the flow is given in Figure 2. The time-averaged graph [Figure 2(a), right-hand side] shows impellers that mainly pump in the radial direction with a small downward inclination. The average axial flow that is induced varies per axial compartment. The lowest

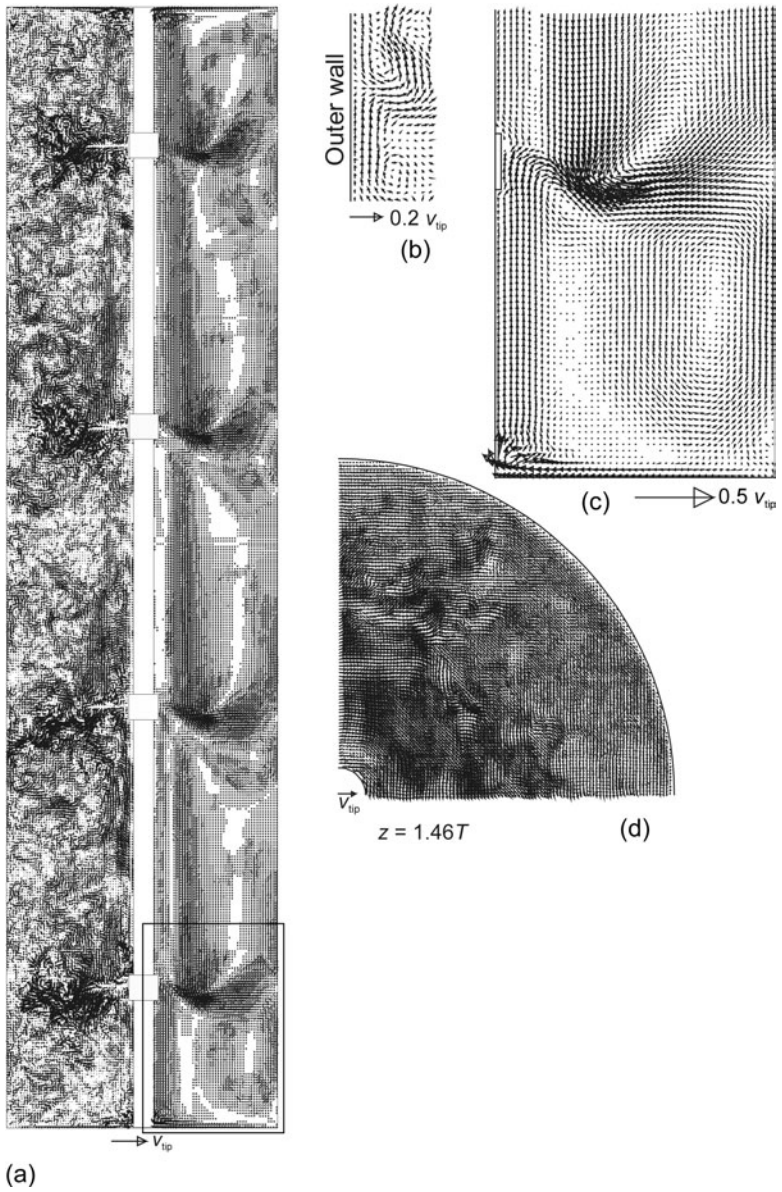

Figure 2. Impressions of the simulated fluid flow in the tank (a) Vertical cross section with left a snapshot of the flow in terms of velocity vectors, and right the time-averaged flow. (b) A zoomed-in snapshot at the outer wall showing a vortex pair known as Taylor–Görtler vortices. (c) The average flow in the lower part of the tank [enlargement of the section in the rectangle in (a)]. (d) A horizontal cross section (snapshot) at $z = 1.46\ T$, i.e., slightly below impeller #2.

compartment (the region underneath impeller #1) has upflow near the shaft, and downflow near the outer wall [see also Figure 2(c)]. In the next compartment (in between impeller #2 and #1) there is a very weak upflow near the shaft. At larger radii, there is downflow. Eventually, at the outer wall fluid moves in the upward direction again, except for the upper part of this compartment where the jet emerging from impeller #2 hits the outer wall. This jet induces a recirculation at an axial level slightly below impeller #2 that forces fluid in the downward direction close to the outer wall. For the compartments between impeller #3 and #2, and between #4 and #3 a similar picture applies, except that the upflow very close to the shaft is virtually absent here. The compartment above impeller #4 contains a single, big recirculation with downflow near the shaft and upflow near the outer wall. In the boundary layers attached to the top and bottom end-walls, fluid moves with high velocity inwardly [Figure 2(c)]. This strong radial flow is due to the radial pressure gradient induced by the swirl. Outside the boundary layers the radial pressure gradient is balanced by centrifugal forces. Inside the boundary layer, however, the tangential velocity is strongly reduced and centrifugal forces are much weaker; the pressure gradient takes over and forces fluid inwardly (Ekman boundary layers). The strongly swirling motion of the fluid is manifest in Figure 2(d). Another typical feature of swirling flow is the occurrence of Taylor–Görtler vortices (Escudier *et al.*, 1982). These are vortex pairs near a concave solid wall. In between the two vortices forming the pair fluid moves in the negative radial direction [see Figure 2(b)].

The way the impeller acts is further detailed in Figure 3, which shows angle-resolved averaged velocity fields in the vicinity of impeller #2. The impeller forms a double tip vortex (the formation of tip vortices in unbaffled vessels

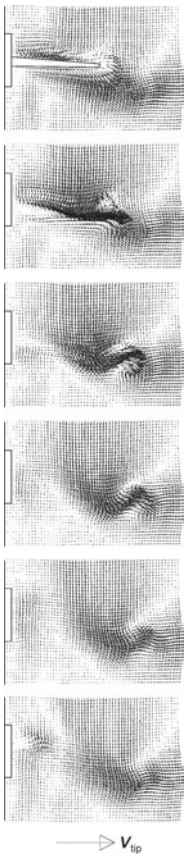

Figure 3. Impeller-angle-resolved average flow in a vertical plane in the vicinity of impeller #2. the orientation of an impeller blade relative to the plane of view is (from top to bottom) 0°, 20°, 40°, 60°, 80°, 100°.

was reported earlier by Sharp and Adrian, 2001; Alcamo *et al.*, 2005), the upper one being much stronger than the lower one. The impeller outstream meanders in between these two vortices directly induced by the blade and a third steady vortex at the axial level of the impeller and with its center at approximately at $r = 0.29T$ (this steady vortex is also visible on the phase-averaged fields shown in Figure 2).

PARTICLE MOTION MODELLING

Our main interest was in modelling the motion of solid particles that were released in the tank operating at $Re = 1.6 \times 10^5$. Given the fact that a single-phase simulation of one impeller revolution takes about 7 hours of wall-clock time when running in parallel on 12 CPUs, resolving the experimentally observed particle migration to the top of the tank which happened on a $10^4/N$ timescale needs some sort of modelling (just running the code long enough for the particles to reach the top would mean running it for some 8 years).

The modelling idea that was applied consisted of releasing the particles in a sequence of previously stored single-phase flow fields. The particles then feel the spatial and temporal variations present in the flow. The extent to which they feel the variations depends on the resolution with which the flow information is stored, and on the length of the stored time series. An important limitation of the method is that we are not able to include particle-to-fluid coupling effects (two-way coupling) since the method is based on previously calculated flow fields of which the particle behaviour is *a priori* not known.

The tank has an axisymmetric geometry (no baffles). Therefore, the relevant circumferential coordinate from the perspective of a solid particle immersed in the flow is its angular position relative to the impeller. For this to capture we only need to store a sequence of flow fields in a single, vertical half-plane of the tank. This gives us a representation of the flow in an axial-radial plane at a specific angle relative to the impeller. Since we store a sequence of these planes, all planes have their specific position relative to the impeller. This we use to build a three-dimensional flow field, which is a function of axial, radial, and tangential position, where the tangential positions runs over 2π times the number of impeller revolutions that we store. This three-dimensional field satisfies continuity just as the original Cartesian flow fields. Only using a sequence of data from a single plane clearly is a simplification (instigated by limited memory of computers). In what follows the consequences of the simplification will be assessed.

Stepping the particle motion in time now goes as follows: suppose a particle has velocity $\mathbf{v}_p$, then during one time step Δt the particle moves over the vector $\mathbf{v}_p \Delta t$. In the radial and axial direction this respectively is $v_{pr}\Delta t$ and $v_{pz}\Delta t$. In the tangential direction next to the contribution $v_{p\theta}\Delta t$ we also have a contribution from the impeller rotating over an angle $\Omega \Delta t$ (if in an inertial frame of reference the particle is standing still, its angular position relative to the impeller increases with an amount $\Omega\ \Delta t$ per time step). The new angular position of a particle relative to the impeller becomes

$$\theta_{p,new} = \theta_{p,old} + \Omega \Delta t - \frac{v_{p^\theta}}{r_p} \Delta t \tag{1}$$

with r_p the radial position of the particle.

The axial-radial planes that we store have the full spatial resolution of the LES. Per lattice-node in the axial-radial plane the three velocity components, the pressure, and the eddy-viscosity (ν_e) value are stored. The latter is used to estimate the RMS values of the subgrid-scale (SGS) velocities (u_{sgs}) according to the relation (Mason and Callen, 1986)

$$u_{sgs} = \sqrt{\frac{2}{3}} k_{sgs} \qquad k_{sgs} = C_k \frac{1}{(c_s \Delta)^2} \nu_e \tag{2}$$

with c_s the Smagorinsky constant (related to the Smagorinsky subgrid-scale model) which was set to 0.1, and C_k a constant amounting to 5. The particle motion is linked to the fluid motion through the drag force and the force on the particle due to the pressure gradients in the fluid. In that respect the pressure and SGS velocities are relevant. Pressure gradients (induced by swirl) may significantly contribute to the total force acting on the particle. In our particle simulations we only consider the radial component of the pressure gradient force that we furthermore assume to be independent of the tangential coordinate. The drag force on a particle is the result its velocity being different from the fluid velocity at the position of the point particle.

The fluid velocity is composed of a grid-scale (GS) and a SGS part.

The single-phase planar fluid flow field is stored every 20 time-steps, corresponding with an impeller rotation of 3°. The length of the fluid flow time series that we use in the particle motion simulations is mainly limited by the internal memory of the computer that we use to run the particle simulation on. For efficient simulations, the sequence of flow fields needs to fit in internal memory. Previously we have applied a similar procedure for modelling cyclone performance (Derksen, 2003) where we read the (then three-dimensional) fields regularly from disk. The latter operations slowed down the simulations significantly. The computer we used has an internal memory of 2 Gbyte. A single data-plane consists of $nx \cdot nr \cdot 4$ (the '4' stands for the three resolved velocity components, and the RMS value of the SGS velocity; the pressure is considered to be independent of the tangential coordinate and therefore hardly contributes to memory usage) single precision real values (with $nx = 800$ and $nr = 100$), representing 1.28 Mbyte of data. As a result, we can fit approximately 1500 fields in memory. With a reference to the frequency (every 3° of impeller revolution) with which we store the fields these are typically 12 impeller revolutions. In what follows, we checked to what extent the results of the particle motion simulations are influenced by the length of the time sequence, and by the temporal/angular spacing between the successive flow fields.

A total number of M fields will be played repeatedly for simulating the particle motion. Preliminary computations showed that unrealistic particle motion occurs when rewinding from the Mth field to the first field. This is due to the discontinuous flow conditions felt by the particles at this moment. This problem was overcome by storing an extra set of M_a fields directly after the set of M fields. We use these M_a fields to linearly interpolate them with the first M_a fields out of the original set with size M ($M > M_a$). This process is visualized for a velocity time series at a single point in Figure 4. The two fields forming a pair that was linearly interpolated had the same impeller angle. It should be noted that although we generate a smooth time-series, from a principle point of view linear interpolation of two flow fields to build a new one is not allowed because of the non-linearity of the Navier–Stokes equations.

Now that we have built a three-dimensional, time-dependent flow out of a sequence of single realizations of planar flow fields, the way the particles motion is modelled can be explained. We view the particles as identical point particles that do not occupy space and therefore do not mutually collide. Their diameter d_p is only relevant for determining the drag force, and the location at which they collide with the bounding walls (at 0.5 d_p from the wall). The equation of motion that we solve for each particle reads

$$\frac{d\mathbf{v}_p}{dt} = C_D \frac{3}{2}\frac{1}{d_p}\frac{\rho_f}{\rho_p + (1/2)\rho_f}\frac{1}{2}|\mathbf{u} - \mathbf{v_p}|(\mathbf{u} - \mathbf{v}_p) - \frac{1}{\rho_p + (1/2)\rho_f}(\nabla p - \mathbf{g}) \quad (3)$$

with ρ_f and ρ_p the fluid and solid density respectively (the addition of $(1/2)\rho_f$ in the denominators reflects the use of an added mass term). The fluid velocity $\mathbf{u}$ at the position of the particle is composed of a grid-scale (GS) and subgrid-scale (SGS) part. The former is determined from linearly interpolating the fluid velocity at the grid nodes to the particle position. The SGS part is due to a three-dimensional, isotropic Gaussian random process with RMS value u_{sgs} [equation (2)]. The refresh rate of the random process is related to the local, turbulent time scale. The latter is estimated to be

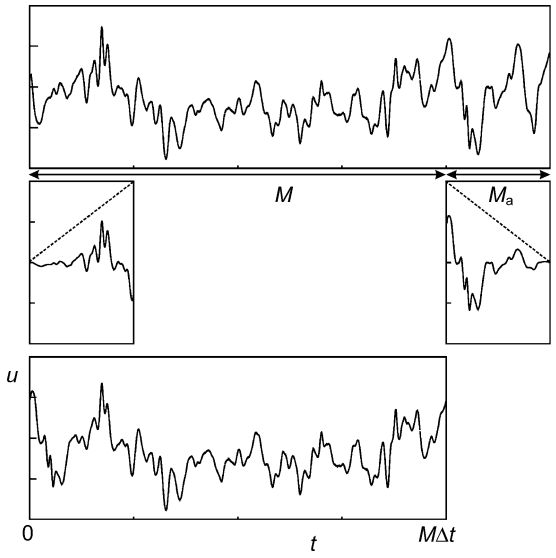

Figure 4. Graphical representation of how we match the beginning and end of a time series in order to make a smooth transition when rewinding the time series. Top: raw time series with length $M + M_a$. Centre: first and last part of the raw time series (both having length M_a) multiplied by linear weighing functions (dashed lines). Bottom: reconstructed time series with the first M_a points now being the sum of the two M_a time series shown in the center graphs.

$$t_{sgs} = C_L \frac{k_{sgs}}{\varepsilon} \quad (4)$$

The constant $C_L = 0.15$. The energy dissipation rate ε is (in the context of the Smagorinsky subgrid-scale model) related to the eddy viscosity: $\varepsilon = \nu_e^3/(c_s\Delta)^4$. For each particle, we renew the random fluid velocity in its vicinity once the time since the last refreshment is larger than the local t_{sgs}.

For the drag coefficient C_D we adopt a non-linear relation that strictly speaking is only valid for a single particle in an unbounded fluid (i.e., we do not take into account the effect of hydrodynamic interaction on drag): $C_D = 24/Re\,(1.0 + 0.15Re^{0.687})$. The second term on the right-hand side of equation (3) represents the force due to a pressure gradient and gravity. The particles collide fully elastically and without friction with the solid boundaries of the flow domain, albeit that particle-impeller collisions hardly occur since the particles preferentially move to the outer wall of the tank.

RESULTS

In order to check if and how the results of the particle simulations depended on the choices made in the modeling, six cases were defined (see Table 1) that had different

Table 1. Characteristics of particle simulations.

Case id	$\Delta\varphi$ (°)	M	Number of revolutions	M_a
Q	6	720	12	60
S	6	1080	18	60
U	3	1440	12	120
V	9	720	18	40
W	6	1440	24	60
X	9	1440	36	40

lengths of the flow time series (M) and/or different temporal/angular spacing ($\Delta\varphi$) between the subsequently stored flow fields. The number of impeller revolutions directly follows from M and $\Delta\varphi$. In every simulation the number of additional flow fields (M_a) to make a smooth wrap-around of the time series (see Figure 4) represented one impeller revolution. The total number of flow fields taking part in the particle simulations was (as explained above) limited by the internal memory of our computer. In what follows, first some impressions of the particle behaviour will be highlighted based on simulations U and W. Subsequently the impact of the numerical settings will be discussed in more detail.

Simulations were started with all 20 000 particles lying randomly scattered on the bottom of the tank, having zero velocity. The particle properties were taken according to the experimental (Pinelli *et al*., 2001) settings: solid over fluid density ratio 2.45, particle size (uniform) $d_p = 0.33$ mm. At $t = 0$ we start playing the series of flow fields in the way that we described above and monitor the particle motion as a result of the fluid flow. A typical evolution is shown in the series of snapshots in Figure 5. In this figure, two different numerical settings (marked as case U and W, see Table 1) are compared. The overall trend is that the particles move towards the upper part of the tank, via a set of ring-shaped, intermediate regions.

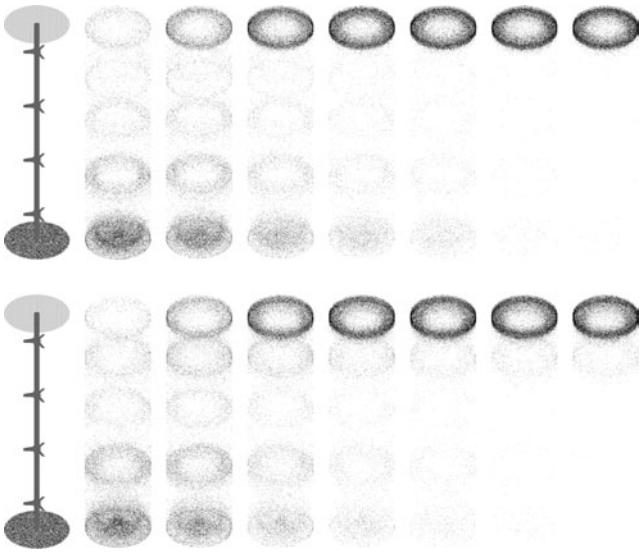

Figure 5. Impression of the evolution of the particle positions in time. Top row: case U (see Table 1); bottom row case W. From left to right: $t = 0$ (all particles lying on the bottom), $t = 10^3/N$, $t = 2 \times 10^3/N$, $t = 4 \times 10^3/N$, $t = 6 \times 10^3/N$, $t = 8 \times 10^3/N$, $t = 14 \times 10^3/N$, $t = 18 \times 10^3/N$ (corresponding to 18 min).

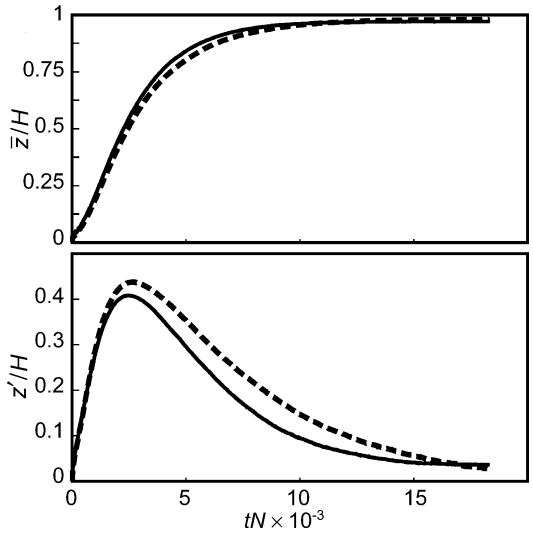

Figure 6. Time series of the mean vertical particle position (top) and its standard deviation (bottom) from simulation cases U (dashed) and W (drawn).

These rings correspond to regions that have downflow near the outer wall [see Figure 2(a)]. What happens is that particles move up in the compartment below impeller #1 and get caught in the impeller stream emerging from impeller #1. From now on, swirl confines the particles mostly to the outer part of the tank. Here, the fluid velocity in the z-direction is mainly positive, except for four (ring shaped) regions at the wall, at impeller level. The particles escape from these rings by turbulent fluctuations. In this respect it is essential to have a sufficiently long flow time series that has a large enough repertoire of fluctuations (releasing the particles in a single, frozen flow field would probably confine them to the recirculation zones forever). Eventually almost every particle ends up in the compartment above impeller #4. A steady particle field is reached after approximately 15 000 impeller revolutions, corresponding to 15 min. This very well corresponds to the experimental observations (Pinelli *et al*., 2001) that report 20 min to a steady state particle field. The time series in Figure 6 of the mean axial particle position $\bar{z}$, and the RMS value z' (defined as $z' = \sqrt{(1/(n-1)\sum(z_i^2 - \bar{z}^2)}$ where the sum is over all n particles) show the gradual rise of the particles, and a maximum spreading of particles over the column at $t \approx 3000/N$.

The steady state vertical particle concentration profiles for cases U and W are shown in Figure 7, along with the experimental profile (Pinelli *et al*., 2001). The simulated profiles have been obtained by counting all particles that were within a certain height range during a time interval of $1600/N$. We see that the simulated profiles are much sharper than the experimentally observed one. We will discuss this discrepancy in the subsequent section.

Sensitivity to Numerical Settings

In modelling the long-time particle motion, we essentially have to make two choices: the time (or angular) spacing between the subsequently stored single-phase flow fields ($\Delta\varphi$ in Table 1), and the length of the flow's time series (e.g., in terms of the number of impeller revolutions).

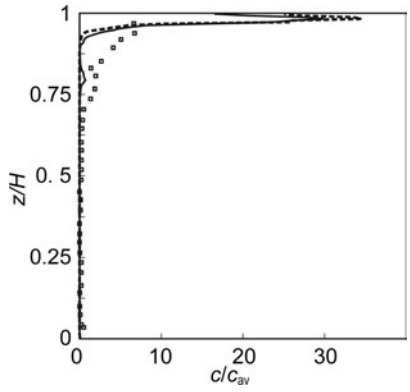

Figure 7. Time-averaged vertical solids concentration profiles from simulation cases U (dashed), and W (drawn), and from the experiments of Pinelli *et al*. (2001) (symbols). In the simulations, time averaging was started once the particle fields reached steady state.

In this section we check how these choices influence the particle behaviour in terms of the time it takes for the particles to reach a steady state in the top of the tank, and in terms of the steady state vertical concentration profiles.

As can be seen, the spacing between the fields hardly influences the results. In Figure 8 we compare a spacing of $\Delta\varphi = 3^\circ$ and 6° for a time-span of 12 revolutions, in Figure 9 a spacing of $\Delta\varphi = 6^\circ$ and 9° for a time span of 18 revolutions. Hardly any influence of the angular spacing on the particle behavior can be observed. This is not the case for the length of the time series: this parameter clearly has its impact on the particle motion (Figure 10). In terms of the vertical concentration profiles: they get slightly wider for longer time series. Furthermore, for the 24 and 36 impeller revolution series (cases W and X), the profiles exhibit a secondary maximum at a level slightly below impeller #4 (in qualitative agreement with the experimental data, see Figure 7). The minor differences between cases W and X suggest that a fluid flow time series of 24 revolutions is sufficient for the results to become insensitive of the length of the flow time series. In view of the rise time of the particles, however, this is not the case: in case X (36 revolutions flow time series) particles rise much quicker than in case W (24 revolutions flow time series). The latter is probably due to the larger repertoire of flow

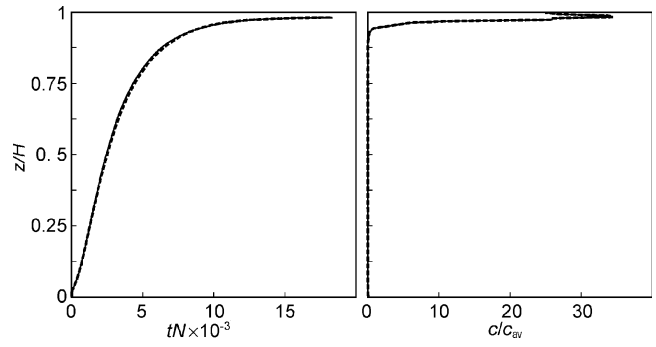

Figure 8. Left: time evolution of the average vertical particle position for case Q (dashed) and U (drawn). Right: time-averaged vertical solids concentration profiles from simulation cases Q (dashed), and U (drawn).

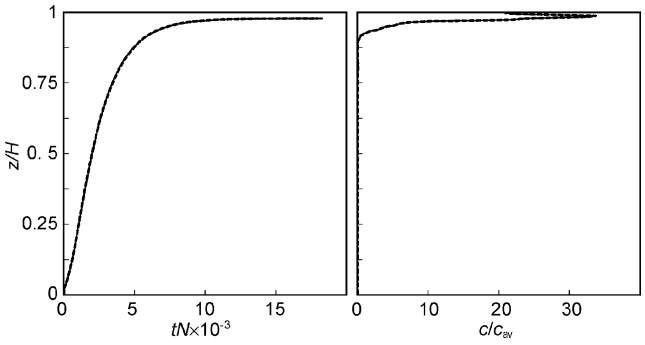

Figure 9. Left: time evolution of the average vertical particle position for case S (dashed) and V (drawn). Right: time-averaged vertical solids concentration profiles from simulation cases S (dashed), and V (drawn).

realizations in case X, making it more likely for particles to escape from the intermediate ring-shaped regions on their way to the top.

In all the simulations there seems to be a lack of dispersion: the particle concentration profiles are much narrower than their experimental counterpart (see Figure 7). Extending the length of the fluid flow time series is not going to help much in this respect (see Figure 10, and the discussion above). Since apparently the grid-scale fluid velocity is not dispersing the particles sufficiently, we investigated the impact of the strength of the subgrid-scale fluid motion on the concentration profiles. This was done by increasing the constant C_k [Equation (2)] by a factor of 16 (four times higher u_{sgs}), and 100 (10 times higher u_{sgs}) and observing how this affects the concentration profiles. The results in Figure 11 indicate a clear effect; increasing u_{sgs} by a factor of 10 gives a profile with a width comparable to the experimental one. It is not very likely, however, that our estimates of k_{sgs} are off by a factor 100 (u_{sgs} by a factor of 10).

To further check our modelling, we also investigated the consequences of the simplification involved in sampling the flow in a single, vertical half-plane. We did this by taking a single realization of the particles from simulation X at $t \approx 1.4 \times 10^4/N$ (i.e., in quasi steady state, see Figure 10) and releasing the particles in the full three-dimensional flow field. We subsequently simulated the

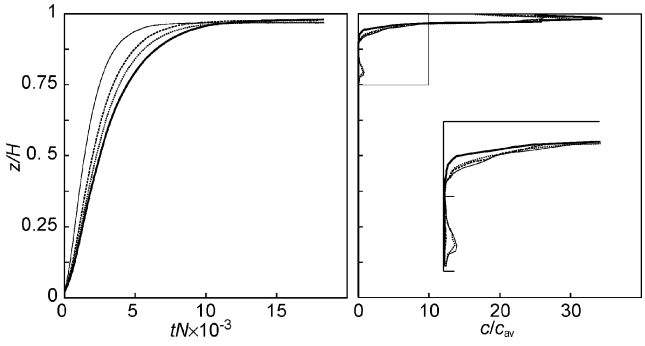

Figure 10. Left: time evolution of the average vertical particle position for case Q (thick, drawn), S (dashed), W (dotted), and X (thin, drawn). Right: time-averaged vertical solids concentration profiles from the same simulations. The inset corresponds to the rectangle in the upper-left corner of the right graph.

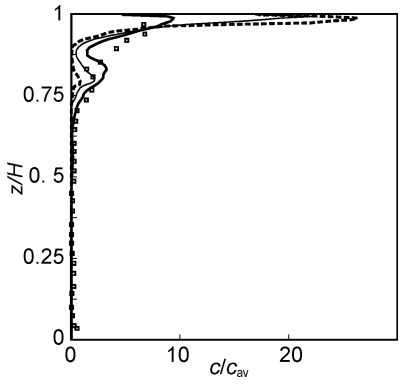

Figure 11. Time-averaged vertical solids concentration profiles from case X with variation of the subgrid-scale velocities. Original data (dashed), four times higher u_{sgs} (drawn, thin), 10 times higher u_{sgs} (drawn, thick), and the experiments of Pinelli *et al.* (2001) (symbols).

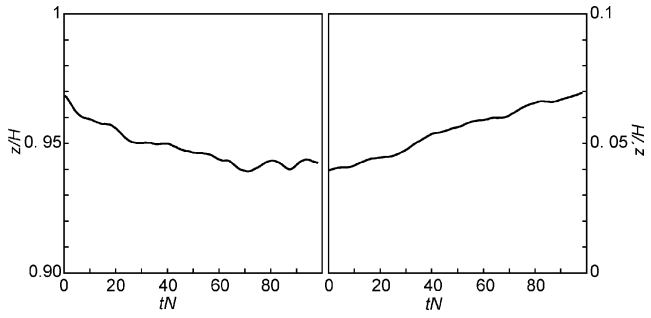

Figure 12. Concurrent simulation of fluid flow and particle motion. Left: time evolution of the average vertical particle position; right: time evolution of the RMS value of the vertical position.

concurrent motion of fluid and particles under one-way coupling assumptions during almost 100 impeller revolutions (this simulation was computationally more expensive than all previously presented simulations together). The results in terms of the average axial particle position and its and RMS value are given in Figure 12 (please note that the time-scale of this figure is very small compared to the previously reported time series). We initially see a slight decrease of the average position. After 75 impeller revolutions it stabilizes. The RMS value, however, keeps increasing continuously over the nearly 100 simulated revolutions, indicating that compared to the simulations of Table 1 a broader repertoire of fluid fluctuations is felt by the particles in a concurrent simulation. Figure 13 displays the solids volume fraction profile at the end of the concurrent simulation (i.e., after almost 100 impeller revolutions).

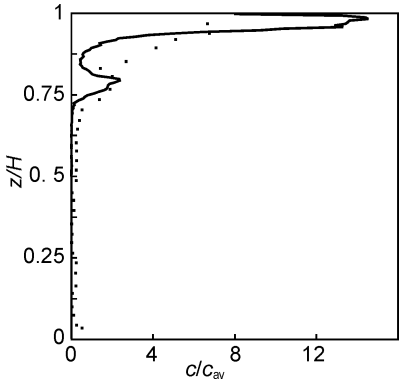

Figure 13. Vertical solids concentration profile retrieved from the concurrent simulation after almost 100 impeller revolutions (drawn line), and the experiments of Pinelli *et al.* (2001) (symbols).

CONCLUSIONS

In this paper we have outlined a strategy for the use of large-eddy simulations for processes that span many (here of the order of 10^4) integral time scales of the flow. In such situations, running the LES over the entire time span is not an option because it would take too much computer time (on present-day computers). As an alternative we have suggested the use of a previously stored flow time series that is repeatedly played and in which the process (particle dispersion in this paper, but it also could have been a chemically reacting system, or a liquid–liquid dispersion) is carried out. The advantage of this approach is that we make use of the highly resolved flow information in the LES. The approach is, however, not universal: Since we carry out the flow simulation prior to the actual process, the method does not allow for back-coupling, i.e., the fluid flow does not sense the process (here it does not feel the presence of the solid particles). Furthermore, the method is memory intensive. In the example discussed here this was less of a limitation since the unbaffled tank had an axisymmetric geometry and we could to a large extent limit ourselves to storing flow information in a single plane. In fully three-dimensional geometries data volumes (as opposed to data planes) need to be stored.

The specific problem that was discussed here was the distribution of solid particles in a tall, unbaffled tank equipped with four A310 impellers showing experimentally (Pinelli *et al.*, 2001) counterintuitive behaviour: almost all particles rise to the top of the tank. The migration from bottom to top took place in approximately 20 min, corresponding to of the order of 10^4 impeller revolutions. The fluid flow simulations showed a strongly swirling flow with Ekman layers at the end-walls and Taylor–Görtler vortices. In the absence of baffles, the pumping action of the A310 impellers was mainly in the radial direction.

The centrifugal force induced by the swirl drives particles (with a density larger than the fluid density) towards the outer wall. Since at the outer wall the main flow direction is upward, particles gradually rise to the top of the tank. In this process turbulent dispersion is essential since at some vertical stages along the outer wall downflow obstructs the (on average) upward motion of the particles. The total time it takes for the particles to migrate from bottom to top corresponds with the experimentally observed process time. The simulated steady-state particle concentration profiles, however, are significantly sharper than their experimental counterparts. Concurrent, three-dimensional simulations of fluid flow and particle motion tended to more realistic particle concentration profiles (however at dramatically higher computational cost). We therefore conclude that the schematization of the flow time series (with flow information confined to planes instead of volumes) that was made to keep the

computations tractable in terms of computer memory usage limits the accuracy of the proposed procedure in this strongly three-dimensional flow system.

An additional reason for the observed deviation could be the inaccurate estimate of the subgrid-scale kinetic energy emerging from the (simple) Smagorinsky model. It was demonstrated that the steady-state particle concentration profiles are definitively sensitive to subgrid-scale fluctuation levels: Artificially increasing the subgrid-scale velocities by a factor of 10 while keeping the resolved velocities unaffected significantly broadens the steady-state particle concentration profile. Proper estimation of subgrid-scale motion is therefore essential to the proposed method. In this respect, it would be beneficial to revisit the experiment and measure next to particle concentration fields fluid flow velocities (average values and fluctuations levels) to see which part of the modelling described here (SGS modelling of the flow, particle motion modelling, planar fields) most urgently requires improvement.

REFERENCES

Alcamo, R., Micale, G., Grisafi, F., Brucato, A. and Ciofalo, M., 2005, Large-eddy simulation of turbulent flow in an unbaffled stirred tank driven by a Rushton turbine, *Chem Eng Sci*, 60(8–9): 2303–2316.

Bakker, A. and Oshinowo, L.M., 2004, Modelling of turbulence in stirred vessels using large eddy simulation, *Trans IChemE, Part A, Chem Eng Res Des*, 82(A9): 1169–1178.

Baldyga, J., Bourne, J.R., Pacek, A.W., Amanullah, A. and Nienow, A.W., 2001, Effects of agitation and scale-up on drop size in turbulent dispersions: allowance for intermittency, *Chem Eng Sci*, 56: 3377–3385.

Chen, S. and Doolen, G.D., 1998, Lattice Boltzmann method for fluid flows, *Ann Rev Fluid Mech*, 30: 329–364.

Derksen, J.J. and Van den Akker, H.E.A., 1999, Large eddy simulations on the flow driven by a Rushton turbine, *AIChE J*, 45: 209–221.

Derksen, J.J. and Van den Akker, H.E.A., 2000, Simulation of vortex core precession in a reverse-flow cyclone, *AIChEJ*, 46: 1317–1331.

Derksen, J., 2001, Assessment of large eddy simulations for agitated flows, *Trans IChemE, Part A, Chem Eng Res Des*, 79A: 824–830.

Derksen, J.J., 2003, Separation performance predictions of a Stairmand high-efficiency cyclone, *AIChE J*, 49: 1359–1371.

Derksen, J.J., 2005, Simulations of confined turbulent vortex flow, *Comput Fluids*, 34: 283–299.

Escudier, M.P., Bornstein, J. and Maxworthy, T., 1982, The dynamics of confined vortices, *Proceedings Royal Society London*, A382: 335–360.

Hartmann, H., Derksen, J.J. and Van den Akker, H.E.A., 2004, Macroinstability uncovered in a Rushton turbine stirred tank by means of LES, *AIChE J*, 50: 2383–2393.

Hollander, E.D., Derksen, J.J., Portela, L.M. and Van den Akker, H.E.A., 2001, A numerical scale-up study for orthokinetic agglomeration in stirred vessels, *AIChE J*, 47: 2425–2440.

Kramer, H.J.M. and Jansens, P.J., 2003, Tools for design and control of industrial crystallizers—state of the art and future needs, *Chem Eng Tech*, 26: 247–255.

Kraume, M., Gabler, A. and Schulze, K., 2004, Influence of physical properties on drop size distributions of stirred liquid-liquid dispersions, *Chem Eng Tech*, 27: 330–334.

Mason, P.J. and Callen, N.S., 1986, On the magnitude of the subgrid-scale eddy coefficient in large-eddy simulations of turbulent channel flow, *Journal of Fluid Mechanics*, 162: 439–462.

Montante, G., Micale, G., Magelli, F. and Brucato, A., 2001, Experiments and CFD predictions of solid particle distribution in a vessel agitated with four pitched blade turbines, *Trans IChemE, Part A, Chem Eng Res Des*, 79(A8): 1005–1010.

Pinelli, D., Nocentini, M. and Magelli, F., 2001, Solids distribution in stirred slurry reactors: influence of some mixer configurations and limits of the applicability of a simple model for predictions, *Chemical Engineering Communications*, 188: 91–107.

Smagorinsky, J., 1963, General circulation experiments with the primitive equations: 1. The basic experiment, *Monthly Weather Review*, 91: 99–164.

Roussinova, V., Kresta, S.M. and Weetman, R., 2003, Low frequency macroinstabilities in a stirred tank: scale-up and prediction based on large eddy simulations, *Chem Eng Sci*, 58: 2297–2311.

Sharp, K.V. and Adrian, R.J., 2001, PIV study of small-scale flow structure around a Rushton turbine, *AIChE J*, 47: 766–778.

Van Vliet, E., Derksen, J.J. and Van den Akker, H.E.A., 2005, Turbulent mixing in a tubular reactor: assessment of an FDF/LES approach, *AIChE J*, 51: 725–739.

ACKNOWLEDGEMENTS

I would like to thank Dr André Bakker who brought the flow system considered here to my attention, and who showed a keen and active interest in the results, and Prof. Franco Magelli and Dr Giuseppina Montante for their advice and feedback.

The manuscript was received 15 March 2005 and accepted for publication after revision 25 October 2005.